ISPRS Annals of the Photogrammetry, Remote Sensing and Spatial Information Sciences, Volume X-5/W2-2025
Unleashing the power of Geospatial & Frontier Technologies for a Sustainable Future – GIFTS Summit 2025,
1–3 September 2025, Symbiosis International University, Pune, India

Spatial Mapping of Saltwater Intrusion in Coastal Odisha, India using Hydrochemical Signatures and Machine Learning Tools

Suhani Srujanika[1*], Rasika Masare[1], Payal Waindeshkar[1], Amit V. Shirke[1], Prabhu Prasad Das[2], Bhavana Umrikar[1]

1. Department of Geology, Savitribai Phule Pune University, Pune- 411017
2. Department of Geology, Dharani Dhar University, Keonjhar- 758001

E-mail ID: s.srujanika@gmail.com

Keywords: Groundwater chemistry, salinity, machine learning, RF, coastal aquifers, Odisha, India.

Abstract

Freshwater resources in coastal regions are increasingly at risk of salinization as a result of seawater intrusion, posing serious challenges to source sustainability. This study introduces a systematic approach for delineating vulnerable zones through hydrogeochemical assessment integrated with spatial and machine learning techniques. To demarcate the extent of contamination, groundwater samples were collected from 33 tubewells of Ersama block, Odisha during both pre and post-monsoon seasons of 2023, key ionic constituents such as Cl^-, HCO_3^-, and Na^+ were analysed. Two critical hydrochemical ratios, Cl^-/HCO_3^- and Na^+/Cl^- were computed to quantify the level of salinization and to distinguish the sources of salinity respectively. Based on established threshold values, contamination levels were categorized into six classes, which were further refined by combining them with salinity origin to form 11 hybrid classes. These hybrid classes were used as labelled categories for classification using the Random Forest (RF) algorithm. Spatial distribution of classified zones was visualized using ArcGIS, enabling effective identification of contaminated areas. During the pre-monsoon, zones classified as high to extreme contamination due to seawater intrusion accounted for 19.1% of the area, while other sources contributed 31% in the same severity range. In the post-monsoon, seawater-related contamination showed a notable decrease to 6.4%, whereas contamination from other sources significantly elevated to 43%. This suggests a seasonal dilution effect on saline water intrusion immediately after monsoon due to the reversal of hydraulic gradient, though contamination from non-marine sources intensified. This approach offers a practical and scalable solution for monitoring saltwater intrusion dynamics in coastal settings.

1. Introduction

Groundwater forms the backbone of freshwater supply in many coastal regions, supporting both agricultural and domestic needs. However, the sustainability of this vital resource is increasingly under threat due to a complex interplay of natural and anthropogenic factors. Among the most pressing concerns is seawater intrusion (SWI), a process where saline water from the sea infiltrates freshwater aquifers, leading to a gradual deterioration in water quality. This issue is particularly acute in coastal aquifers, which are in direct hydraulic connection with the sea and are simultaneously exposed to pollutants from urban, agricultural, and industrial sources (Sethi et al., 2014; Panda et al., 2021; Manivannan et al., 2022; Barik et al., 2021; Jena et al., 2024; Das et al., 2020).

Globally, the phenomenon of SWI is well-documented and is typically linked to excessive draft of fresh groundwater, which creates inland hydraulic gradients that facilitate the encroachment of seawater into freshwater aquifers. This process is further accelerated by rising sea levels, unregulated pumping for agriculture, and declining recharge due to urbanization (FAO, 1997). In Odisha, several studies have confirmed the issue of SWI and related salinization, not only due to marine influence but also from land-based sources such as shrimp pond infiltration, domestic wastewater, and natural mineral dissolution (Das et al., 2016; Barik et al., 2021). The coastal stretch of Jagatsinghpur district, has long been identified as a zone vulnerable to saline water ingress and associated land degradation. Several blocks in this district experience chronic problems like saline soils, waterlogging, and reduced crop productivity, which are compounded by groundwater over-extraction and limited recharge. In fact, certain areas have already been declared as salinity-affected zones where further groundwater development is officially restricted (Sethi et al., 2014). Further, the surface and near-surface water are contaminated by frequent cyclones and flooding episodes.

Understanding the geochemical nature of salinity is crucial for differentiating between marine and non-marine sources. Classical studies, such as those by Revelle (1941) and Simpson (reported in Todd, 1959), have established that chloride (Cl^-) concentration and specific ionic ratios, particularly $Cl^-/(CO_3^{2-} + HCO_3^-)$ and Na^+/Cl^-, can serve as indicators of saline intrusion. In seawater-dominated systems, a low Na^+/Cl^- ratio and a high Cl^-/HCO_3^- ratio are typically observed (Jones et al., 1999; Moujabber et al., 2006), whereas elevated Na^+/Cl^- ratios (>1) often signal influence from anthropogenic sources, such as sewage or fertilizer runoff. Furthermore, deviations from simple seawater–freshwater mixing are often noted due to rock-water interactions, ion exchange, or contamination by subsurface brines (Appelo and Geirnaert, 1991; Vengosh and Rosenthal, 1994; Sudaryanto and Naily, 2018).

Although the hydrogeochemical behavior of saline intrusion is relatively well understood, a key gap in current research lies in the integration of geochemical parameters with data-driven modeling techniques. Recent advancements in machine learning (ML), particularly ensemble-based classifiers like Random Forest, offer promising tools for handling complex environmental datasets and classifying spatially heterogeneous conditions (Kushwaha et al., 2024; Kim et al., 2024). However, the application of such techniques in the context of saltwater intrusion management in coastal Odisha remains limited. As highlighted by recent literature, there is a pressing need to combine hydrogeochemical insight with computational

This contribution has been peer-reviewed. The double-blind peer-review was conducted on the basis of the full paper.
https://doi.org/10.5194/isprs-annals-X-5-W2-2025-671-2025

intelligence to produce reliable spatial models that can inform groundwater management (Asare et al., 2021; Srivastava et al., 2013).

In this context, the present study focuses on the Ersama block in Jagatsinghpur district, aiming to assess the extent of SWI, distinguish between marine and non-marine sources of salinization, and generate seasonal vulnerability maps using a combined approach. By applying Cl^-/HCO_3^- and Na^+/Cl^- ratios, followed by classification through a Random Forest algorithm, the study attempts to delineate hybrid contamination zones and assess seasonal dynamics in salinity patterns. This integrative framework is expected to provide a more nuanced understanding of contamination processes and support sustainable groundwater development in coastal areas facing similar threats.

2. Study area

The present study is focused on the Ersama block, situated within the Jagatsinghpur district of Odisha, along the eastern coastal plain of India (Figure 1). This region forms part of the southern delta of the Mahanadi basin, characterized by extensive Quaternary alluvial deposits with a complex and dynamic depositional history. The area lies within the Mahanadi-Devi interfluve, where sedimentation processes over geological time have given rise to a highly heterogeneous subsurface environment.

Geologically, the subsurface stratigraphy of the region is marked by alternating granular and non-granular horizons, forming a diverse lithological framework (Shukla, 2011; Das et al., 2016a; Das et al., 2018; Das et al., 2020). The granular units, comprising sands and gravels of varying grain sizes, serve as the primary aquifers, while non-granular layers, dominated by silts and clays, act as aquitards or confining beds. The presence of fossiliferous layers, lateritic crusts, and heavy mineral bands further points to the region's dynamic sedimentological evolution. This alternating arrangement of permeable and impermeable layers results in multi-aquifer systems, where freshwater and saline water zones often occur in close proximity, both vertically and laterally, with no distinct hydrogeological boundaries separating them.

The study area is underlain by two major geological Formations: the Burhabalang Formation and the Bankigarh Formation. The Burhabalang Formation contains significant marine sediments, indicative of its depositional environment, whereas the Bankigarh Formation is primarily composed of floodplain deposits, often incorporated with calcareous nodules (Das et al., 2020). These Formations together contribute to the region's unique hydrostratigraphic set-up, influencing both the availability and quality of groundwater.

Climatically, the area falls under the humid subtropical zone, experiencing hot summers, a wet monsoon period, and cool winters (Naik, 2018). The months of May and June are typically the hottest, with daytime temperatures soaring up to 40°C. Annual rainfall is substantial, predominantly occurring during the southwest monsoon season, which plays a significant role in aquifer recharge processes. The region exhibits a dendritic drainage pattern, reflecting the maturity of the fluvial landscape. Numerous palaeo-channels and abandoned river courses further illustrate the dynamic hydrological evolution of the delta.

The Taladanda Canal, an important irrigation infrastructure fed by the Mahanadi River, plays a crucial role in meeting the agricultural, industrial, and domestic water demands of the area. However, the dependence on canal water and shallow groundwater sources, especially in the background of increasing salinity and tidal ingress, raises concerns about long-term water security and the need for sustainable groundwater management practices. Given its unique geological setup, dynamic salinity patterns, and growing water demand, the Ersama block presents a representative site for assessing saltwater intrusion and for testing integrated approaches to classify and monitor groundwater vulnerability in coastal aquifers.

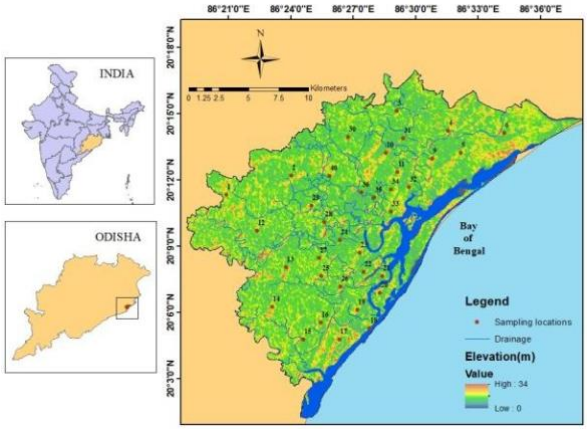

Figure 1: Study area map showing the sampling locations

3. Methodology

The issue addressed in the present study is the contamination of coastal aquifers due to SWI and other salinizing processes. The central aim is to determine whether an integrated hydrogeochemical and data-driven approach can effectively identify and classify the contamination zones, particularly in a dynamic deltaic setting like the Ersama block. In this context, the objectives defined for the investigation are:

(1) To undertake a detailed hydrogeochemical assessment of groundwater using key ionic ratios to evaluate both the extent and origin of salinity;

(2) To delineate contamination zones by classifying the severity and source of salinization through an integrated approach combining hydrochemical indicators and machine learning techniques; and

(3) To evaluate the seasonal variability of saline intrusion by comparing spatial patterns of contamination between pre- and post-monsoon periods, with the aim of understanding the dynamics of groundwater quality under changing hydrological conditions.

3.1 Data collection and In-situ measurements

Groundwater sampling was systematically carried out in the Ersama block during the pre-monsoon and post-monsoon seasons of 2023, with site selection guided by variations in geology, topography, hydrology, and anthropogenic influence. A total of 33 representative tubewells of varying depths were selected across the study area to capture spatial and seasonal variability in groundwater chemistry. The geographical coordinates of each sampling location were recorded using a Garmin handheld GPS device (Model ETREX 20) to ensure precise spatial referencing for subsequent GIS-based analysis.

Field measurements of pH, electrical conductivity (EC), and total dissolved solids (TDS) were performed on-site using a Combo pH/Conductivity/TDS Tester (Hanna HI98130, High Range). Water samples were collected in acid-cleaned polypropylene bottles. Prior to sampling, bottles were rinsed with 1:1 nitric acid (HNO_3) followed by multiple washes with distilled water to eliminate any residual contaminants.

Following collection, groundwater samples were immediately filtered through 0.2 µm nylon filters to remove suspended particulates. Each filtered sample was then divided into two aliquots: One aliquot was acidified to pH < 2 using concentrated HNO_3 for cation analysis. The second aliquot was left unacidified for anion and alkalinity determination. Samples were stored in a cold box during fieldwork and later transferred to a refrigerator in the laboratory to maintain chemical stability until analysis.

3.2 Laboratory analysis

All geochemical analyses were conducted following established analytical protocols (Samanta et al., 2019; Rout and Tripathy, 2024). Groundwater alkalinity was determined using an autotitrator (Metrohm Titrino Plus 877). Major cations (Ca^{2+}, Mg^{2+}, Na^+, K^+) and anions (Cl^-, SO_4^{2-}, NO_3^-) were analyzed using an ion chromatograph (Metrohm Compact IC Plus 882) at the Indian Institute of Science Education and Research (IISER), Pune.

The analytical accuracy and precision were maintained within ~4%, as verified through replicate analysis of selected samples and by using certified reference standards from Merck for both cations and anions. The reliability of analytical data was further evaluated through the Normalized Inorganic Charge Balance (NICB), calculated using the formula:

$$NICB = 100 \times [(TZ^+ - TZ^-) / ((TZ^+ + TZ^-)/2)], \quad (1)$$

where TZ^+ and TZ^- represent the total equivalents of cations and anions, respectively. The NICB values for all samples averaged within ±5% (n = 33), indicating a high level of analytical accuracy and consistency.

3.3 Pre-processing of Data for Machine Learning Model

A series of pre-processing steps were conducted to prepare the hydrogeochemical data for machine learning classification and ensure the dataset been accurate, interpretable, and appropriate for predictive modeling. As a first step, two key hydrochemical ratios were derived from the major ion concentrations: the chloride-to-bicarbonate ratio (Cl^-/HCO_3^-) and the sodium-to-chloride ratio (Na^+/Cl^-). The Cl^-/HCO_3^- ratio, often referred to as Simpson's ratio, served as a reliable indicator of salinity and potential SWI (Todd, 1959; Vengosh et al., 1997). This ratio was used to classify the groundwater samples into six contamination levels based on widely accepted threshold values. (Table 1). Further distinction was achieved using the Na^+/Cl^- ratio, which enabled the identification of the salinity source. Ratios below 0.85 were interpreted as strong evidence of marine origin, whereas values above 0.85 suggested non-marine sources, such as anthropogenic activities or natural geochemical processes (Jones et al., 1999) (Table 2).

The contamination categories derived from the Cl^-/HCO_3^- values were combined with the salinity origin indicated by the Na^+/Cl^- ratio, with the exception of the uncontaminated water/ clean water (Class 0), creating a hybrid classification system to enable supervised learning. This merged approach produced 11 unique hybrid classes, which were then encoded into numerical labels suitable for training a machine learning model (Table 3).

Cl^-/HCO_3^- Ratio	Water Quality Level	Class no.
< 0.5	Good	0
0.5 – 1.3	Slightly Contaminated	1
1.3 – 2.8	Moderately Contaminated	2
2.8 – 6.6	Highly Contaminated	3
6.6 – 15.5	Very Highly Contaminated	4
> 15.5	Extremely Contaminated	5

Table 1: Classification of Water Quality Based on Cl^-/HCO_3^- Ratio

Na^+/Cl^- Ratio	Inferred Salinity Source	Class
≤ 0.85	Marine (Seawater Intrusion)	Marine
> 1	Terrestrial/Anthropogenic	Non-marine

Table 2: Classification of Salinity Source Based on Na^+/Cl^- Ratio

Subsequently, the Random Forest (RF) classifier was employed due to its robustness against overfitting and its ability to model complex, non-linear relationships. The RF model was trained using 80% of the Cl^-/HCO_3^- and Na^+/Cl^- ratios as input features and the numeric hybrid classes as target variables. The ensemble method, which constructs multiple decision trees using bootstrapped subsets of the dataset and random feature selection, proved to be highly effective in capturing the variability within the groundwater dataset. The model achieved notable predictive accuracy, reaching up to 90% on the 20% testing data, highlighting its potential as a powerful tool for groundwater quality classification in coastal settings. (earlier, Chitra madam recommended 70:30)

Class No.	Cl^-/HCO_3^- Contamination Level	Na^+/Cl^- Inferred Source	Hybrid Class Label
0	Good (< 0.5)	Not Applicable	0_Good water
1	Slightly Contaminated	Non-marine	1_Non-marine
2	Moderately Contaminated	Non-marine	2_Non-marine
3	Highly Contaminated	Non-marine	3_Non-marine
4	Very Highly Contaminated	Non-marine	4_Non-marine
5	Extremely Contaminated	Non-marine	5_Non-marine
6	Slightly Contaminated	Marine	6_Marine
7	Moderately Contaminated	Marine	7_Marine
8	Highly Contaminated	Marine	8_Marine
9	Very Highly Contaminated	Marine	9_Marine
10	Extremely Contaminated	Marine	10_Marine

Table 3: Hybrid Classification of Groundwater Based on Contamination Levels and Salinity Sources

After training, the model was saved for further applications. Classified results were integrated with spatial coordinates of the sampling locations and visualized in QGIS, allowing the generation of predictive maps delineating zones of different contamination levels and salinity sources.

3.4 Geospatial analysis

Geospatial analysis was employed as a core component to understand the spatial dynamics of groundwater contamination and potential marine influence. All geospatial processing and mapping were carried out using ArcGIS (version 10.8), a GIS platform that enabled effective integration of hydrochemical and machine learning algorithms with spatial coordinates.

The field sample locations, each associated with Cl^-/HCO_3^- and Na^+/Cl^- ratios, as well as the final hybrid class predictions generated through the Random Forest classifier, were first georeferenced using their GPS-derived coordinates. These data were then overlaid onto base layers that included administrative boundaries and drainage network for visual analysis.

The pointwise discrete groundwater quality data was converted into continuous spatial surfaces by applying the Inverse Distance Weighting (IDW) interpolation. IDW was chosen for its simplicity and its proven efficiency in handling relatively sparse datasets typical of hydrogeological field studies (Watson and Philip, 1985). The interpolated raster datasets represented variations in contamination levels (as per Cl^-/HCO_3^- value) and source indicators (as per Na^+/Cl^- value), helping delineate zones of marine and non-marine salinity impact across the study area. In addition, the hybrid classes (ranging from Class 1 to Class 10), which integrated both the intensity and source of contamination, were also spatially visualized.

4. Results and Discussion

The present investigation focuses on the evaluation of major ionic constituents in groundwater samples and examines their spatial and seasonal variability across the coastal aquifer systems. The following results are discussed by integrating physicochemical parameters, hydrochemical ratios, machine learning classifications, and spatial patterns, enabling a multi-faceted output. Given the complexity and variability observed in groundwater chemistry, the discussion has been structured to highlight seasonal trends, contamination gradients, and the marine vs. non-marine sources of salinity, thereby offering insights into the controlling processes behind SWI and aquifer vulnerability.

4.1 Physicochemical Characterization of Groundwater

The physicochemical profile of groundwater across the study area reveals considerable spatial and seasonal variability, reflecting the dynamic interactions between freshwater and saline sources. Total Dissolved Solids (TDS) exhibited a broad range, particularly during the pre-monsoon (PRM) season, with concentrations spanning from 225.85 mg/L to 24,054.92 mg/L and averaging 1,895.92 mg/L. In the post-monsoon (POM) period, TDS values were slightly lower, ranging from 108.94 mg/L to 25,177.16 mg/L, with a mean of 1,673.37 mg/L. Notably, Electrical Conductivity (EC), a key indicator of salinity, peaked at over 37,500 µS/cm in PRM and 39,000 µS/cm in POM, suggesting significant saltwater intrusion, particularly in coastal locations such as Garh Kujanga in the Ersama block.

Groundwater pH varied seasonally as well, with slightly acidic to near-neutral conditions observed. During PRM, pH values ranged between 5.0 and 7.2 (mean: 6.2), while in POM, the range shifted to 5.8-7.9, with a mean of 6.6. The relatively lower pH during PRM could be attributed to increased dissolved CO_2 from intruding saline water, which forms carbonic acid, thereby lowering the pH, a mechanism aligned with prior findings (Barker & Ridgwell, 2012).

	pH	TDS (mg/L)	EC (µS/cm)	Na (meq/l)	K (meq/l)	Ca (meq/l)	Mg (meq/l)	Cl (meq/l)	NO3 (meq/l)	SO4 (meq/l)	HCO3 (meq/L)
Pre-monsoon											
Min	5.0	225.85	352.89	1.93	0.07	0.08	0.15	1.29	0.01	0.12	0.50
Max	7.2	24054.92	37585.82	260.71	3.41	82.25	77.57	423.86	2.25	6.26	9.23
Mean	6.2	1895.92	2962.37	21.19	0.54	6.40	4.60	26.80	0.50	1.52	4.08
Post-monsoon											
Min	5.8	108.94	170.21	0.70	0.00	0.27	0.56	0.95	0.02	0.00	0.49
Max	7.9	25177.16	39339.31	281.76	6.04	82.87	80.93	406.07	1.11	31.92	9.01
Mean	6.6	1673.37	2614.64	16.32	0.67	6.18	5.86	22.09	0.21	2.28	3.68

Table 4: Statistics of hydrochemical ions in the study area

In terms of major cations, the dominance order was consistent in both seasons as $Na^+ > Ca^{2+} > Mg^{2+} > K^+$. Sodium was the most prevalent, with concentrations ranging from 1.93 to 260.71 mEq/L in PRM and 0.70 to 281.76 mEq/L in POM, reflecting its prominent role in saline groundwater environments. The average sodium levels also dropped from 21.19 mEq/L in PRM to 16.32 mEq/L in POM, possibly due to dilution effects post-

monsoon. Magnesium levels were elevated in both seasons, with mean values of 4.60 mEq/L (PRM) and 5.86 mEq/L (POM), and maximum concentrations exceeding 77 mEq/L, further supporting the influence of marine ingress.

Among the anions, the sequence of prevalence was $Cl^- > HCO_3^- > SO_4^{2-} > NO_3^-$. Chloride, a key marker of seawater contamination, exhibited substantial concentrations, ranging from 1.29 to 423.86 mEq/L in PRM and 0.95 to 406.07 mEq/L in POM, with seasonal averages of 26.80 mEq/L and 22.09 mEq/L, respectively. Sulphate levels, which are often influenced by both natural and anthropogenic sources, recorded averages of 1.52 mEq/L in PRM and 2.28 mEq/L in POM, with a notable post-monsoon spike possibly linked to agricultural runoff or domestic effluents (Brindha et al., 2017; Deepa & Venkateswaran, 2018; Adimalla and Qian, 2019).

Nitrate, though present in relatively low concentrations, ranged from 0.01 to 2.25 mEq/L in PRM and 0.02 to 1.11 mEq/L in POM, with means of 0.50 mEq/L and 0.21 mEq/L, respectively, values that generally fall within WHO (2017) guidelines for potable water, though localized anthropogenic inputs cannot be ruled out. Additionally, increase in the TDS values in post-monsoon season in some samples reciprocate to increase in potassium, magnesium, and sulphate concentrations that can be attributed to enhanced mineral dissolution, agricultural runoff, and intensified water-rock interactions following seasonal recharge.

4.2 Hydrochemical indicators

Specific hydrochemical indicators have been utilized to understand the extent and influence of marine intrusion on the coastal groundwater system . These indicators are particularly useful in identifying subtle shifts in water chemistry that signal salinization processes.

Among these, Electrical Conductivity (EC) serves as a fundamental parameter in showcasing the groundwater type. EC values showed a wide seasonal variation, with some samples recording extremely high values up to 37,586 µS/cm during the pre-monsoon and 39,339 µS/cm in the post-monsoon period (High ranges for both the seasons). Since EC reflects the total ionic concentration of water, elevated values often indicate the presence of dissolved salts originating from marine sources. According to Karahanoglu (1997), groundwater samples with EC values exceeding 3000 µS/cm are considered indicative of seawater influence. Samples ranging between 2000 and 3000 µS/cm represent brackish water conditions, while those with EC below 2000 µS/cm are generally classified as freshwater (Manivannan et al., 2022). In the current study, around 12% to 15% of groundwater samples exceeded 3000 µS/cm threshold, pointing to marine intrusion, while another 12% to 15% fell within the brackish range, and about 70% to 75% remained within freshwater limits (Table 5).

Another significant diagnostic tool is the Simpson's Ratio, expressed as $Cl^- / (HCO_3^- + CO_3^{2-})$. This ratio is particularly effective in tracing marine intrusion, as chloride is abundant in seawater whereas bicarbonate and carbonate are typically low. An increasing ratio reflects a growing dominance of marine water in the groundwater mixture. Based on established classification, values below 0.5 indicate good quality water, 0.5-1.3 signify slight contamination, 1.3-2.8 moderate contamination, 2.8-6.6 high contamination, 6.6-15.5 very high contamination and values exceeding 15.5 denote extremely contaminated water (Moujabber et al., 2006).

Classes based on EC	Percentage of samples on pre-monsoon (%)	Percentage of samples on post-monsoon (%)
Fresh water	69.69	75.76
Brackish water	15.15	12.12
Saline water	15.15	12.12

Table 5: Statistics of samples based on EC values

During the pre-monsoon season, a very small percentage of samples (just over 3%) were classified as good quality, with low Cl^-/HCO_3^- ratios. Most samples showed signs of contamination, with about 30% falling into the slightly contaminated category, 24% classified as moderately contaminated, and around 27% showing high contamination levels. A smaller fraction, roughly 9%, fell into the very highly contaminated class, and 6% of samples exhibited extremely contaminated, indicating severe salinity influence. In the post-monsoon season, there was a slight shift toward improved water quality. The proportion of good-quality samples doubled to around 6%, while the share of highly contaminated samples dropped significantly. However, the percentage of moderately and slightly contaminated samples increased, suggesting that monsoonal recharge might have diluted highly saline zones but did not eliminate salinity-related issues entirely (Table 6).

Classes based on Cl^-/HCO_3^-	Percentage of samples on pre-monsoon (%)	Percentage of samples on post-monsoon (%)
Good	3.03	6.06
Slightly contaminated	30.30	36.36
Moderately contaminated	24.24	27.27
Highly contaminated	27.27	15.15
Very-highly contaminated	9.09	9.09
Extremely contaminated	6.06	6.06

Table 6: Statistics of samples based on Cl^-/HCO_3^- values

The Na^+/Cl^- molar ratio offers insight into the origin of salinity. In natural seawater, this ratio is close to 0.86. Values below this threshold typically indicate direct seawater mixing, while ratios greater than one may reflect anthropogenic inputs or ion exchange processes (Jones et al., 1999; Vengosh & Rosenthal, 1994).

The data indicate a marked seasonal shift in Na^+/Cl^- ratios. During the pre-monsoon season, the majority of samples—nearly 70%—displayed ratios greater than 0.86, suggesting that most groundwater was influenced by non-marine sources. However, post-monsoon, this percentage dropped significantly to about 52%. Nearly 48% of the samples during the post-monsoon showed Na^+/Cl^- ratios below 0.86, which implies a broader spread of seawater influence after the monsoon period.

This contribution has been peer-reviewed. The double-blind peer-review was conducted on the basis of the full paper.
https://doi.org/10.5194/isprs-annals-X-5-W2-2025-671-2025 | © Author(s) 2025. CC BY 4.0 License.

Classes based on Na^+/Cl^-	Percentage of samples on pre-monsoon (%)	Percentage of samples on post-monsoon (%)
Non-marine sources	69.70	51.52
Marine sources	30.30	48.48

Table 7: Statistics of samples based on Na^+/Cl^- values

4.3 Spatial Distribution and Interpretation of Hybrid Hydrochemical Classes

The hybrid classification approach integrated two critical hydrochemical indicators, namely the Cl^-/HCO_3^- ratio (to assess contamination severity) and the Na^+/Cl^- molar ratio (to infer the potential source of salinity, i.e., marine or non-marine). This resulted in eleven distinct hybrid classes (Class 0 to Class 10), each representing a unique combination of contamination level and salinity origin.

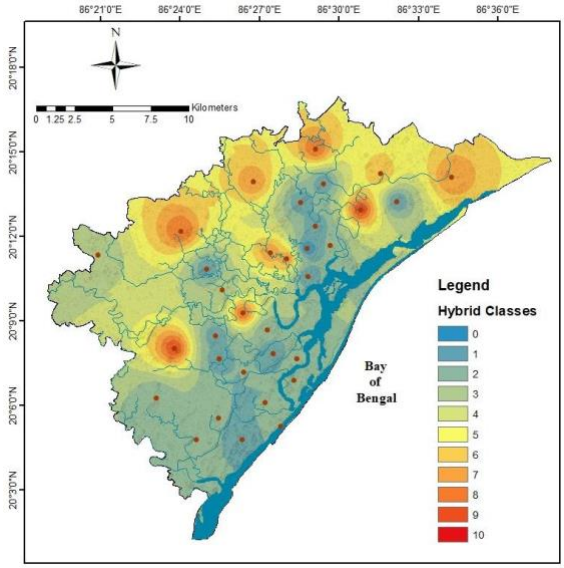

Figure 2: Spatial distribution of hybrid classes during pre-monsoon season

The spatial distribution maps for pre- and post-monsoon seasons (Figure 2 & 3) reveal a distinct variation in the extent and severity of contamination across the region. During the pre-monsoon period, non-marine classes (Classes 1 to 5) collectively accounted for over 62.4% of the area, with Class 2 (moderately contaminated, non-marine) alone occupying the highest proportion (21.8%), followed by Class 3 (18.8%). Meanwhile, marine-influenced classes (Classes 6 to 10) covered 37.3%, with Class 8 (very highly contaminated, marine) showing significant spatial presence at 12.5%, particularly around the coastal and creek-adjacent zones (Figure 4).

In the post-monsoon season, a marked shift is observed in the classification pattern. The non-marine classes reduced to 63.6%, and although Classes 1 to 3 showed a slight decline, there was a substantial increase in Class 4 (very highly contaminated, non-marine), rising to 19.8% from just 7.1% in the pre-monsoon period. Interestingly, the spatial extent of Class 6 (slightly contaminated, marine) expanded significantly to 18.2%, indicating a deeper inland movement of marine signatures. However, the most highly saline marine classes (8 to 10) showed a general reduction, possibly influenced by dilution or recharge effects from the monsoon (Figure 5).

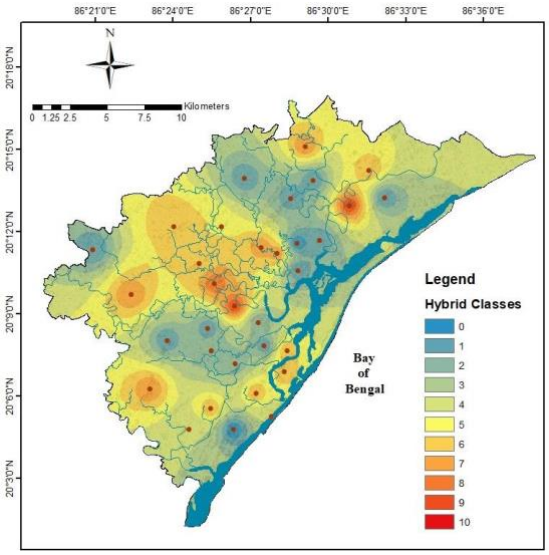

Figure 3: Spatial distribution of hybrid classes during post-monsoon season

It is essential to interpret these spatial patterns carefully. The higher hybrid classes in the eastern and southeastern parts of the region, especially Classes 8 and 9, are aligned with proximity to the Bay of Bengal, suggesting strong marine influence likely through lateral intrusion. However, the possibility of vertical migration due to deeper marine layers cannot be overlooked, especially in the absence of depth-specific data. Therefore, these patterns should not be exclusively interpreted as lateral contamination without considering aquifer depth variability.

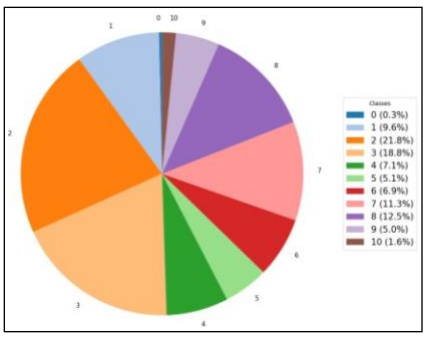

Figure 4: Pie-chart depicting the percentage of area occupied by each hybrid class in pre-monsoon season

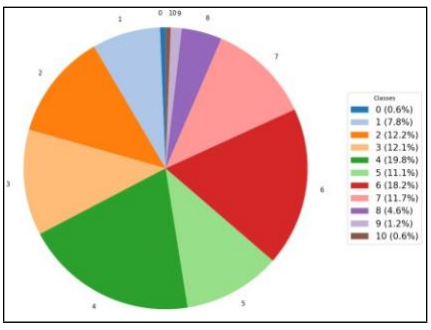

Figure 5: Pie-chart depicting the percentage of area occupied by each hybrid class in post-monsoon season

Moreover, several inland pockets exhibiting non-marine salinity (Classes 1 to 5) near creek systems could be attributed to anthropogenic influences, such as seepage from shrimp aquaculture ponds. The recurrence of these hybrid classes around such land uses underscores the potential role of land-based saline water sources in driving localized groundwater degradation.

Overall, the hybrid classification method and the generated random forest model offers a nuanced view of the spatio-seasonal evolution of groundwater salinity, highlighting both natural and human-induced salinization processes. This classification serves as a critical diagnostic tool for groundwater managers aiming to devise targeted intervention strategies in vulnerable zones in the future.

5. Conclusion

The present study is focused on a comprehensive evaluation of saltwater intrusion and salinization patterns in the coastal aquifers from parts of East India, integrating hydrochemical indicators, spatial interpolation, and a hybrid classification variable. Seasonal analysis revealed significant variations in salinity levels, with post-monsoon conditions showing a relative intensification of non-marine salinity sources, potentially driven by anthropogenic activities such as seepage from shrimp aquaculture ponds. Geochemical ratios of Cl^-/HCO_3^- and Na^+/Cl^-, proved to be effective in discerning the degree and origin of contamination, while the hybrid classification provided a more refined interpretation by capturing both contamination severity and source influence. Spatial patterns indicated not only lateral saline intrusion near the coast but also hinted at possible vertical migration, underlining the role of depth as a governing factor that warrants further investigation. This geospatial framework not only enabled the identification of vulnerable zones but also laid the groundwork for integrating hydrogeochemical signatures with landscape-level features, essential for framing targeted groundwater management strategies in future studies. In addition to empirical analysis, a machine learning model was developed and tested, achieving an overall accuracy of 90%. This model holds promising as a predictive tool for identifying vulnerable zones and can be further refined for regional-scale groundwater management and early warning systems. Overall, the integrated approach adopted in this study contributes to a more informed understanding of coastal aquifer salinization and supports the design of targeted mitigation strategies.

Acknowledgements

This work was financially supported by the University Grants Commission (UGC), Government of India, through the NET-JRF fellowship. We sincerely thank Dr. Gyana Ranjan Tripathy, Department of Earth Sciences, IISER Pune, for providing access to laboratory facilities essential for the hydrochemical analysis. Further, we thank the reviewers for their suggestions and comments which helped to improve the manuscript.

References

Adimalla, N., Qian, H., 2019. Groundwater quality evaluation using water quality index (WQI) for drinking purposes and human health risk (HHR) assessment in an agricultural region of Nanganur, south India. *Ecotoxicology and Environmental Safety*. 176, 153–161. https://doi.org/10.1016/j.ecoenv.2019.03.066

Appelo, C. A. J., Geirnaert, W., 1991. Processes Accompanying the Intrusion of Salt Water Hydrology of Salt Water Intrusion. Hannover. pp 291–304

Asare, A., Appiah-Adjei, E. K., Ali, B., Owusu-Nimo, F., 2021. Assessment of seawater intrusion using ionic ratios: The case of coastal communities along the Central Region of Ghana. *Environmental Earth Sciences*, 80(8). https://doi.org/10.1007/s12665-021-09601-x

Barik, K. K., Panda, S. R., Nanda, S., Tripathy, J. K., Chhotaray, P. K., Annadurai, R., Mishra, S. P., Mitra, D., 2021. GIS based saltwater vulnerability mapping of the northern coast of Odisha, East coast of India. *Arabian Journal of Geosciences*, 14(14). https://doi.org/10.1007/s12517-021-07800-1

Barker, S., Ridgwell, A., 2012. Ocean Acidification. *Nature Education Knowledge*. 3, 21. https://www.nature.com/scitable/knowledge/library/ocean-acidification-25822734

Brindha, K., Pavelic, P., Sotoukee, T., Elango, L., 2017. Geochemical Characteristics and Groundwater Quality in the Vientiane Plain, Laos. *Expo Health* 9, 89–104. https://doi.org/10.1007/s12403-016-0224-8

Das, P. P., Sahoo, H. K., Mohapatra, P. P., 2016a. Assessing the effects of regional tectonic activity on groundwater flow in a coastal aquifer in India. *Environ Earth Sci*. 75, 1331. https://doi.org/10.1007/s12665-016-6161-9.

Das, P. P., Sahoo, H. K., Mohapatra, P. P., 2016. Hydrogeochemical evolution and potability evaluation of saline contaminated coastal aquifer system of Rajnagar, Odisha, India: A geospatial perspective. *Journal of Earth System Science*, 125(6), 1157–1174. https://doi.org/10.1007/s12040-016-0721-y

Das, P. P., Sahoo, H. K., Mohapatra, P. P., Pattanaik, J. K., Goswami, S., 2018. A review of saline influences on coastal Mahanadi deltaic aquifers. *Vistas in Geological Research*-16, Utkal Uni. Alumni Assoc., Bhubaneswar, pp. 24–34.

Das, P. P., Mohapatra, P. P., Goswami, S., Mishra, M., Pattanaik, J. K., 2020. A geospatial investigation of interlinkage between basement fault architecture and coastal aquifer hydrogeochemistry. *Geoscience Frontiers*, 11(4), 1431–1440. https://doi.org/10.1016/j.gsf.2019.12.008

Deepa, S., Venkateswaran, S., 2018. Appraisal of groundwater quality in upper Manimuktha sub basin, Vellar river, Tamil Nadu, India by using Water Quality Index (WQI) and multivariate statistical techniques. *Modeling Earth Systems and Environment*, 4(3), 1165–1180. https://doi.org/10.1007/s40808-018-0468-3

FAO, 1997. Seawater intrusion in coastal aquifers. *Guidelines for Study Monitoring and Control.* 7–23, 124–150.

Jones, B. F., Vengosh A., Rosenthal, E., Yechieli, Y., 1999: Geochemical Investigations. *Theory and Applications of Transport in Porous Media* (pp. 51–71). Springer Netherlands. https://doi.org/10.1007/978-94-017-2969-7_3

Jena, M. R., Tripathy, J. K., Sahoo, D., Sahu, P., 2024. Geochemical Evaluation of Groundwater Quality in the Coastal Aquifers of Kujang Block, Jagatsinghpur District, Eastern Odisha, India. *Water, Air, & Soil Pollution*, 235(6). https://doi.org/10.1007/s11270-024-07153-x

Karahanoglu, N., 1997. Assessment of sea-water intrusion in a coastal aquifer by using correlation, principal component, and factor analyses. *Water Environ Res.* 69(3):331–341

Kim, J., Ma, Y., Maxwell, R. M., 2024. Integrating groundwater pumping data with regression-enhanced random forest models to improve groundwater monitoring and management in a coastal region. *Frontiers in Water*, 6. https://doi.org/10.3389/frwa.2024.1509945

Kushwaha, N. L., Sushanth, K., Patel, A., Kisi, O., Ahmed, A., Abd-Elaty, I., 2024. Beach nourishment for coastal aquifers impacted by climate change and population growth using machine learning approaches. *Journal of Environmental Management*, 370, 122535. https://doi.org/10.1016/j.jenvman.2024.122535

Manivannan, V., Manoj, S., RamyaPriya, R., Elango, L., 2022. Delineation and quantification of groundwater resources affected by seawater intrusion along the east coast of India. *Environmental Earth Sciences*, 81(10). https://doi.org/10.1007/s12665-022-10418-5

Moujabber, M. E., Samra, B. B., Darwish, T., Atallah, T., 2006. Comparison of Different Indicators for Groundwater Contamination by Seawater Intrusion on the Lebanese Coast. *Water Resources Management*, 20(2), 161–180. https://doi.org/10.1007/s11269-006-7376-4

Naik, P. C., 2018. Seawater Intrusion in the Coastal Alluvial Aquifers of the Mahanadi Delta. *Springer International Publishing*. https://doi.org/10.1007/978-3-319-66511-5

Panda, S. R., Mishra, S. P., Tripathy, J. K., Barik, K. K., 2021. The Failed Resilience, Grim Water Future, and Salinity Intrusion through GIS of Kendrapara Coast, Odisha. 14. 161-181.

Revelle, R., 1941. Criteria for recognition of sea water in ground waters. *Trans. Amer. Geophysical Union*. 22, 593–597.

Rout, R. K., Tripathy, G. R., 2024. Net effect of chemical erosion in a tropical basin on carbon cycle: Constraints from elemental and sulfur isotopic composition of the Mahanadi river water. *Chemical Geology*, 644, 121859. https://doi.org/10.1016/j.chemgeo.2023.121859

Samanta, A., Tripathy, G. R., Das, R., 2019. Temporal variations in water chemistry of the (lower) Brahmaputra River: Implications to seasonality in mineral weathering. *Geochem. Geophys. Geosyst.* 20 (6), 2769–2785.

Sethi, R. R., Kaledhonkar, M. J., Das, M., Srivastava, S. K., Nayak, A. K., Kumar, A., (2023). Groundwater Pumping Options in Coastal Areas of Odisha. *Journal of the Indian Society of Coastal Agricultural Research*, 32(1), 49-53. https://epubs.icar.org.in/index.php/JISCAR/article/view/137121

Srivastava, S. K., Sethi, R. R., Ashwani, K., Srivastava, R. C., Nayak, A. K., 2013. GW development and energy use dynamics for irrigation in Odisha. *Directorate of Water Management*, Research Bulletin No. 56, pp 1–45

Sudaryanto, & Naily, W. (2018). Ratio of Major Ions in Groundwater to Determine Saltwater Intrusion in Coastal Areas. IOP Conference Series: *Earth and Environmental Science*, 118, 012021. https://doi.org/10.1088/1755-1315/118/1/012021

Shukla, N. K., 2011. Geological and Hydrogeological Evaluation of the Coastal Aquifers of Orissa with Special Reference to the North Part of Mahanadi Delta. Ph.D. thesis, Utkal University, p. 259.

Todd, D. K., 1959. Ground water hydrology. United States. *John Wiley and Sons*. Inc. pp 277–294.

Vengosh, A., Gill, J., Reyes, A., Thoresberg, K., 1997. A multi-isotope investiga6tion of the origin of groundwater salinity in Salinas valley, California. *American Geophysical Union*, San Francisco, California.

Vengosh, A., Rosenthal, A., 1994. Saline groundwater in Israel: its bearing on the water crisis in the country. *J Hydrol.* 156:389–430. https://doi.org/10.1016/0022-1694(94)90087-6

Watson, D., Philip, G., 1985. A refinement of inverse distance weighted interpolation. *Geo-processing*, Vol. 2, No. 4, pp. 315-327.

WHO, 2017. Guidelines for drinking water quality. 3rd ed. World Health Organization, Geneva.